New Physics: Sae Mulli,
Vol. 70, No. 1, January 2020, pp. 24∼28
http://dx.doi.org/10.3938/NPSM.70.24

D^*-Meson Photoproduction off the Proton Target with the Regge Contribution

Seung-il Nam*
Department of Physics, Pukyong National University (PKNU), Busan 48513, Korea
Center for Extreme Nuclear Matters (CENuM), Korea University, Seoul 02841, Korea
Asia Pacific Center for Theoretical Physics (APCTP), Pohang 37673, Korea

(Received 01 October 2019 : revised 29 October 2019 : accepted 30 October 2019)

We investigate the four individual photoproduction channels off the proton target, corresponding to the isospin single and triplet charmed baryons, $\gamma p \to D^{*0}\Lambda_c^+$ and $\gamma p \to (D^{*+}\Sigma_c^0, D^{*0}\Sigma_c^+, D^{*-}\Sigma_c^{++})$. In this work, we estimate the unpolarized total cross sections as guidance for possible future J-PARC experiments. For this purpose, we employ the effective Lagrangian approach at the tree-level Born approximation with the t-channel D and D^* meson Reggized propagators. In addition, phenomenological form factors are taken into account for considering the spatial extension of the hadrons involved. From the numerical calculations, we observed that cross sections of tens of nanobarns for Λ_c^+ production and a few nanobarns for the Σ_c^{++} ones, which are in the detectable range of cross sections in presently available high-energy experiments.

PACS numbers: 13.60.Rj, 13.60.−r, 13.75.Jz, 14.20.−c
Keywords: Charm production, Photoproduction, Y_c baryon, D meson, Regge trajectory

I. INTRODUCTION

Hadron physics is believed to be governed by the nonperturbative features of quantum chromodynamics (QCD). It explains the generation of hadrons from quarks and gluons in nontrivial manners: confinement, spontaneous breakdown of chiral symmetry, $U(1)$ axial anomaly, and so on. Although QCD as the first principle of strong interactions reveals its significance via lattice-QCD simulations, its direct applications to low-energy regime has not yet been fully understood. To overcome this situation for hadron physics, various effective models were developed based on symmetries, such as the gauge, chiral, and flavor for instance.

Among those low-energy models, to investigate the productions of hadrons from high-energy scattering experiments, the effective Lagrangian approach have been widely employed theoretically. This is based on effectively constructed Lagrangians which represent interacting Yukawa vertices by satisfying symmetries and invariances in strong interaction. Moreover, instead of quarks and gluons which are the QCD degrees of freedom, hadronic degrees of freedom are used at the scale of $\Lambda \approx 1.0$ GeV, being close to the nucleon mass. One of the most phenomenological ingredients of this kind of approach must be various form factors, corresponding to the spatial extension of hadrons.

In the present work, we are interested in the photoproductions of heavy hadrons, which contain the heavier charm quarks, D^*, Λ_c, and Σ_c, i.e., $\gamma p \to D^* Y_c$, where the charmed hyperons $Y_c \sim udc$. These production processes are very similar to the K^*Y photoproduction with the light hyperons $Y \sim uds$. Although charmed hadrons have their own symmetries, such as the spin symmetry, leading to the heavy-quark effective field theory (HQEFT), the significant differences between the Y and Y_c photoproductions in terms of the effective Lagrangian approach are basically the relative strong-coupling constants and cutoff masses for the form factors. Except for them, we can simply employ the theoretical framework employed in our previous work [9].

All the numerical calculations are performed at the tree-level Born approximation with the t-channel D and

*E-mail: sinam@pknu.ac.kr

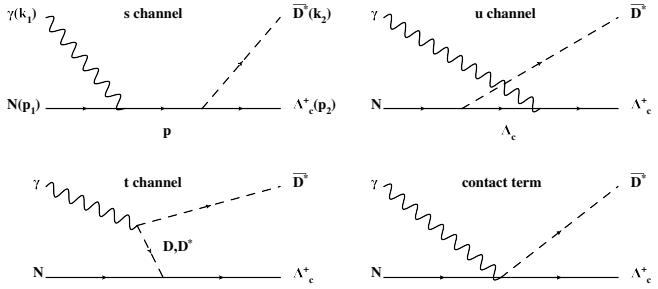

Fig. 1. Relevant Feynman diagrams for the $\gamma N \to \bar{D}^* \Lambda_c^+$ processes. Note that we also define the four momenta for each particle, involved. As for the Σ_c photoproductions, one can use these diagrams similarly, considering the electric charges of the final state.

D^* meson Reggized propagators. The relevant strong coupling constants are taken from the Nijmegen potential model using the flavor SU(4) symmetry relation. As a first trial, we present the numerical results for unpolarized total cross sections for the photoproductions.

II. THEORETICAL FRAMEWORK

In this Section, we make a brief interpretation on the theoretical formalism to study the $\gamma N \to \bar{D}^* \Lambda_c^+$ reaction process. In Fig. 1, we depict the relevant Feynman diagrams for the present reaction process. There, we also indicate the for momenta of the particles involved. As understood from the figure, we take into account the s, u, and t channel contributions, in addition to the contact term, which is necessary to conserve the gauge invariance of the scattering amplitude. First, we define the electromagnetic interactions with the hadrons as follows:

$$\begin{aligned}
\mathcal{L}_{\gamma NN} &= -\bar{N}\left[e_N \not{A} - \frac{e_Q \kappa_N}{4M_N}(\sigma \cdot F)\right] N, \\
\mathcal{L}_{\gamma DD} &= e_D \left[D(\partial_\mu \bar{D}) - \bar{D}(\partial_\mu D)\right] A^\mu, \\
\mathcal{L}_{\gamma DD^*} &= g_{\gamma DD^*} \epsilon_{\mu\nu\sigma\rho}(\partial_\mu A_\nu)(\partial_\sigma D^*_\rho) D + \text{h.c.}, \\
\mathcal{L}_{\gamma D^* D^*} &= i e_{D^*}\left[D^{*\nu}\bar{G}_{\mu\nu} - \bar{D}^{*\nu} G_{\mu\nu}\right] A^\mu,
\end{aligned} \tag{1}$$

where N, A, D, and D^* denote the nucleon, photon, charmed pseudoscalar meson ($D^{\pm,0}$), and charmed vector meson ($D^{*\pm,0}$), respectively. e_h and M_h stand for the electric charge and mass for a hadron h, whereas e_Q unit electric charge. κ_N indicates the anomalous magnetic moment for the nucleon. We define the antisymmetric tensor $\sigma_{\mu\nu} = i(\gamma_\mu\gamma_\nu - \gamma_\nu\gamma_\mu)/2$, using the simplified notation $\sigma \cdot F \equiv \sigma_{\mu\nu}F^{\mu\nu}$. The pseudoscalar-to-vector transition coupling constant $g_{\gamma DD^*}$ can be determined using the experimental data for the corresponding decay widths [4]:

$$\begin{aligned}
\Gamma_{D^{*0}\to D^0\gamma} &< (0.8 \pm 0.06)\,\text{MeV}, \\
\Gamma_{D^{*\pm}\to D^+\gamma} &= (1.54 \pm 0.384 \pm 0.352)\,\text{KeV}.
\end{aligned} \tag{2}$$

Employing these experimental values, one can compute the strengths for the couplings as $g_{D^{*0}D^0\gamma} < 3.42/\text{GeV}$ and $g_{D^{*+}D^+\gamma} \approx 0.153/\text{GeV}$.

As for the strong vertices. we write the interactions as follows:

$$\begin{aligned}
\mathcal{L}_{D^*NY_c} &= -\bar{Y}_c\left[g_{D^*NY_c}\not{D}^* \right. \\
&\quad \left. - \frac{g^T_{D^*NY_c}}{2(M_N + M_{Y_c})}(\sigma \cdot G)\right] N + \text{h.c.}, \\
\mathcal{L}_{DNY_c} &= -i g_{DNY_c}\bar{Y}_c\gamma_5 D N + \text{h.c.}, \\
\mathcal{L}_{\gamma D^* NY_c} &= -\frac{e_{D^*} g^T_{D^*NY_c}}{2(M_N + M_{Y_c})}\bar{Y}_c(\sigma \cdot G')N + \text{h.c.}.
\end{aligned} \tag{3}$$

Here, Y_c denotes the charmed spin-1/2 hyperon. The field-strength tensor for the D^* is assigned as $G_{\mu\nu} = \partial_\mu D^*_\nu - \partial_\nu D^*_\mu$, whereas its gauged one $G'_{\mu\nu} = iA_\mu D^*_\nu - iA_\nu D^*_\mu$. The strong couplings are extracted from the Nijmegen potential model (NSC97a) [8], using the flavor $SU(4)$ relation:

$$g_{DNY_c} = \frac{3 - 2\alpha_D}{\sqrt{3}} g_{KNY}, \quad g_{D^*NY_c} = -\sqrt{3} g_{K^*NY}, \tag{4}$$

where Y stands for the uds-quark hyperon and $\alpha_D \approx 0.64$. Then their values for Λ_c^+ and Σ_c^+ are given in Table. 1.

Table 1. Strong coupling constants for the D^*NY_c and DNY_c vertices, obtained from the Nijmegen potential model (NSC97a) [8] in terms of the flavor SU(4) symmetry.

$g_{D^*N\Lambda_c}$	$g_{D^*N\Sigma_c}$	$g^T_{D^*N\Lambda_c}$	$g^T_{D^*N\Sigma_c}$	$g_{DN\Lambda_c}$	$g_{DN\Sigma_c}$
-4.26	-2.46	-11.31	1.15	-15.80	4.64

The anomalous magnetic momenta of the charmed baryons are listed in Table 2. Those values are taken from the SU(6) quark-model calculations [3].

Table 2. Anomalous magnetic moments for Y_c's in terms of the quark-model calculations [3].

$\kappa_{\Lambda_c^+}$	$\kappa_{\Sigma_c^+}$	$\kappa_{\Sigma_c^{++}}$	$\kappa_{\Sigma_c^0}$
-0.58	-0.55	0.33	-1.44

It is straightforward to compute the invariant amplitudes, which satisfy the Ward-Takahashi identity by construction, using the effective Lagrangians defined above:

$$
\begin{aligned}
i\mathcal{M}_s &= -i\bar{u}_2\left[g_{D^*NY_c}\not{\epsilon}_2 + \frac{g^T_{D^*NY_c}}{M_N+M_{Y_c}}\not{k}_2\not{\epsilon}_2\right] \\
&\quad \left[\frac{\not{k}_1 F_s + (\not{p}_1 + M_N)F_c}{s-M_N^2}\right]\left[e_N\not{\epsilon}_1 + \frac{e_Q\kappa_N}{2M_N}\not{\epsilon}_1\not{k}_1\right]u_1, \\
i\mathcal{M}_u &= -i\bar{u}_2\left[e_{Y_c}\not{\epsilon}_1 + \frac{e_Q\kappa_{Y_c}}{2M_{Y_c}}\not{\epsilon}_1\not{k}_1\right] \\
&\quad \left[\frac{(\not{p}_2 + M_{Y_c})F_c - \not{k}_1 F_u}{u-M_{Y_c}^2}\right] \\
&\quad \left[g_{D^*NY_c}\not{\epsilon}_2 + \frac{g^T_{D^*NY_c}}{M_N+M_{Y_c}}\not{k}_2\not{\epsilon}_2\right]u_1, \\
i\mathcal{M}_{t(P)} &= -g_{\gamma DD^*}g_{DNY_c}\bar{u}_2\gamma_5\mathcal{P}_D u_1\left(\epsilon_{\mu\nu\alpha\beta}k_1^\mu\epsilon^\nu k_2^\alpha\eta^\beta\right)F_v, \\
i\mathcal{M}_{t(V)} &= -ie_{D^*}(k_1\cdot\epsilon_2)\bar{u}_2\mathcal{P}_{D^*}\left[g_{D^*NY_c}\not{\epsilon}_1\right. \\
&\quad + \frac{g^T_{D^*NY_c}}{M_N+M_{Y_c}}(\not{k}_2\not{\epsilon}_1 - \not{k}_1\not{\epsilon}_1 - \epsilon_1\cdot k_2) \\
&\quad \left. - \frac{g_{D^*NY_c}}{M_{D^*}^2}(M_{Y_c}-M_N)(k_2\cdot\epsilon_1)\right]u_1F_c \\
&\quad - 2ie_{D^*}(k_2\cdot\epsilon_1)\bar{u}_2\mathcal{P}_{D^*}\left[g_{D^*NY_c}\not{\epsilon}_2\right. \\
&\quad + \frac{g^T_{D^*NY_c}}{M_N+M_{Y_c}}(\not{k}_2\not{\epsilon}_2 - \not{k}_1\not{\epsilon}_2 + \epsilon_2\cdot k_1) \\
&\quad \left. - \frac{g_{D^*NY_c}}{M_{D^*}^2}(M_{Y_c}-M_N)(k_1\cdot\epsilon_2)\right]u_1F_c \\
&\quad + ie_{D^*}(\epsilon_2\cdot\epsilon_1)\bar{u}_2\mathcal{P}_{D^*}\left[g_{D^*NY_c}\not{k}_2\right. \\
&\quad + \frac{g^T_{D^*NY_c}}{M_N+M_{Y_c}}(\not{k}_2\not{k}_1 - \not{k}_1\not{k}_2) \\
&\quad \left. + \frac{g_{D^*NY_c}}{M_{D^*}^2}(M_{Y_c}-M_N)(k_1\cdot k_2 - k_2^2)\right]u_1F_c, \\
i\mathcal{M}_{\text{contact}} &= ie_{D^*}\bar{u}_2\left[\frac{g^T_{D^*NY_c}}{M_N+M_{Y_c}}\not{\epsilon}_1\not{\epsilon}_2\right. \\
&\quad \left. + \frac{g_{D^*NY_c}}{M_{D^*}^2}(M_{Y_c}-M_N)(\epsilon_1\cdot\epsilon_2)\right]u_1F_c,
\end{aligned}
\tag{5}
$$

Table 3. Slope α' and intercept $\alpha(0)$ for the Regge trajectories for the $D(1870)$ and $D^*(2010)$ mesons [5,6].

	α'	$\alpha(0)$
α_D	$\frac{0.59}{\text{GeV}^2}$	-1.35
α_{D^*}	$\frac{0.50}{\text{GeV}^2}$	-0.86

where the generic and Regge-modified $D^{(*)}$-meson propagators are defined in Eqs. 6 and 7, respectively.

$$
\mathcal{P}_D = \frac{1}{t-M_D^2}, \quad \mathcal{P}_{D^*} = \frac{1}{t-M_{D^*}^2}, \tag{6}
$$

$$
\begin{aligned}
\mathcal{P}_D(s,t) &= \frac{\pi\alpha'_D(1+e^{-i\pi\alpha_D(t)})}{2\Gamma(\alpha_D(t)+1)\sin[\pi\alpha_D(t)]}\left(\frac{s}{s_0}\right)^{\alpha_D(t)}, \\
\mathcal{P}_{D^*}(s,t) &= \frac{\pi\alpha'_{D^*}(1-e^{-i\pi\alpha_{D^*}(t)})}{2\Gamma(\alpha_{D^*}(t))\sin[\pi\alpha_{D^*}(t)]}\left(\frac{s}{s_0}\right)^{\alpha_{D^*}(t)-1}.
\end{aligned}
\tag{7}
$$

The explicit expressions for the relevant four momenta and the polarizations are given in Appendix.

The properties of the Regge trajectories, such as the slope (α') and intercept ($\alpha(0)$) values are depicted in Table 3, using the numerical results from Refs. [5,6].

In order to take into account the spatial extension of the hadrons, it is necessary to consider phenomenological form factors, which guarantees the unitarity of the scattering amplitudes:

$$
\begin{aligned}
F_{s,u,t,v} &= \frac{\Lambda^4}{\Lambda^4 + [(s,u,t,t) - M^2_{N,\Lambda_c,D,D^*}]^2}, \\
F_c &= 1-(1-F_s)(1-F_u)(1-F_t).
\end{aligned}
\tag{8}
$$

Since there have been no experimental data for the present reaction process so far, we choose the cutoff mass for the form factors to be $\Lambda = 0.9$ GeV for all the reaction channels for brevity. Therefore, the numerical results of the cross sections can be used as a qualitative guidance for the future experiments. We also note that these form factor description satisfies the Ward-Takahashi identity at the cross-section level and crossing symmetry of the amplitudes.

III. NUMERICAL RESULTS

In this Section, we provide the numerical results for the total cross sections and differential cross sections as functions of the photon lab. momentum $p_{\text{lab.}}$ and D^*-meson

scattering angle in the cm frame θ_{D^*}, respectively. We also compare the two different cases with and without the Regge modification for the meson propagators. In Fig. 2, we depict the total cross sections with (solid line) and without (dashed line) the Regge modifications. As for $\gamma p \to D^{*0}\Lambda_c^+$, we observe relatively different shapes between the cases: While the curve with the Regge modifications decreases rapidly with respect to the energy beyond the vicinity of the threshold, the one without them does smoothly. The reason for this difference can be understood by that there is no D^*-meson exchange in this channel, due to the electric charge neutrality of the D^{*0} meson in the final state., i.e., the difference between the cures are caused only by the D-meson Regge-modified propagators.

One the contrary, as shown in the panel of $\gamma p \to D^{*-}\Sigma_c^{++}$, there are the D^*-meson exchange in addition to the D-meson one, being different from the previous one. Note that the D^*-meson contribution contains more derivatives in its amplitudes as shown in Eq. 5, the unitarity of the cross section does is not satisfied with the phenomenological form factors in Eq. (8) as far as we address the generic D^*-meson propagator. When, however, the Regge modification turns on for the D^*-meson propagator, the monotonic increase is tamed by the strong suppression from the $(s/s_0)^{\alpha_{D^*}}$ term in Eq. (6). Hence, the validity of the Regge modifications can be explored in future experiments by examining the curve shapes of the cross sections.

From these observations above, one can expect similar tendencies of the cross sections, since the differences among the cases with and without the Regge modifications depend much on the electric charge of the D^* meson in the final state. As expected, we observe similar curves for $\gamma p \to D^{*0}\Sigma_c^+$ with that of $\gamma p \to D^{*0}\Lambda_c^+$, and $\gamma p \to D^{*+}\Sigma_c^0$, with $\gamma p \to D^{*-}\Sigma_c^{++}$, although the strengths of the curves are more or less different, because of the different coupling values as listed in Table 1.

In Fig. 3, we show the numerical results for the differential cross sections in a similar manner with the previous figure. As for $\gamma p \to D^{*0}\Lambda_c^+$, there is a clear difference between the curves with and without the Regge modifications, showing the backward- and forward-scattering enhancements, respectively. Without the modification and

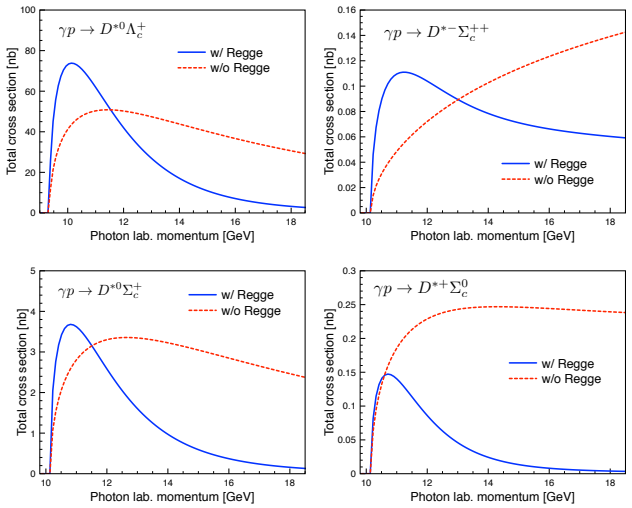

Fig. 2. (Color online) Total cross sections for the $\gamma p \to D^* Y_c$ as a function of the photon lab. momentum $p_{\rm lab.}$ with (solid) and without (dashed) the Regge contributions.

D^*-meson exchange in this channel, the curve shows typical forward-scattering enhancement, due to the strong D-meson t-channel exchange contribution. On the contrary, as the modification takes place, the t-channel exchange gets diminished considerably, resulting in the strong backward-scattering enhancement.

In contrast, turning on the D^*-meson exchange in $\gamma p \to D^{*-}\Sigma_c^{++}$, even for the case without the Regge modification, the curve shows the significant backward-scattering enhancement, whereas the case with it behaves similarly as well. From these observations, we can conclude that in this energy regions beyond the D^*-Y_c threshold, the Regge modifications suppress the t-channel contributions significantly by $(s/s_0)^{\alpha_{D^{(*)}}-J}$, where the $\alpha_{D^{(*)}}$ is negative and J indicates the spin of the exchanging $D^{(*)}$ mesons in the present work. Hence, the s- and u-channel contributions become more visible.

As already observed in the total cross sections in Fig. 2, the curve shapes are much dependent on the electric charge of the outgoing D^* meson, we find similarities even in the differential cross sections as shown in the lower panels of Fig. 3, Although the backward-scattering enhancement becomes weak for $\gamma p \to D^{*+}\Sigma_c^0$, this can be understood by that there is no electric contribution from the u channel, because of the charge neutrality of Σ_c^0. Again, these considerably different curves for the differential cross sections will shed light on testing the present theoretical model.

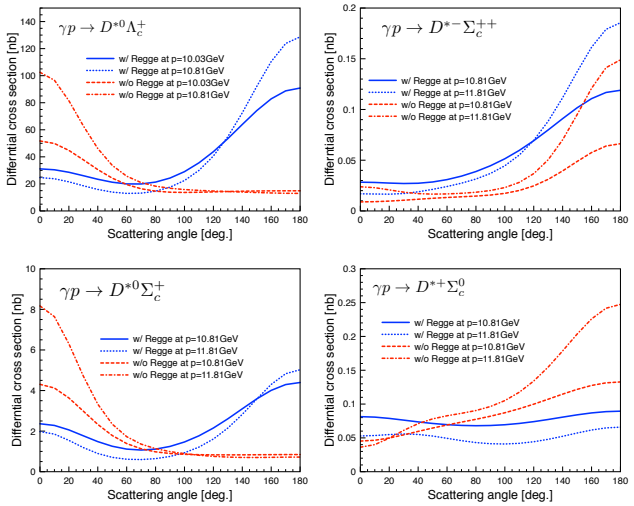

Fig. 3. Differential cross sections $d\sigma/d\cos\theta_{D^*}$ for the $\gamma p \to D^* Y_c$ as a function of the scattering angle θ_{D^*} for the different photon lab momenta.

IV. SUMMARY

In this work, we took into account four individual photoproduction channels off the proton target, corresponding to the isospin single and triplet charmed baryons, $\gamma p \to D^{*0}\Lambda_c^+$ and $\gamma p \to (D^{*+}\Sigma_c^0, D^{*0}\Sigma_c^+, D^{*-}\Sigma_c^{++})$. For this purpose, we employed the effective Lagrangian method with the Regge-modified meson propagators. In addition, the phenomenological form factors were used to tame the monotonic increases with respect to energy. The relevant strong and electromagnetic couplings were taken from available theoretical and experimental information. We observe significant differences between the results with and without Regge contributions, since they suppress the t-channel meson-exchange contributions sufficiently in this energy region $p_{\rm lab} \gtrsim 10$ GeV. With the Regge modifications, we observe rapidly decreasing cross section with respect to the energy and backward-scattering enhancements in the angular distributions. The theoretical differences between them can be settled down by the future experiments. More realistic reactions processes such as three-body Dalitz ones are under investigation and related works will appear elsewhere.

ACKNOWLEDGEMENTS

This work was supported by a Research Grant of Pukyong National University (2017).

APPENDIX

We define the four vectors for the particles in the center-of-mass frame as:

$$\begin{aligned}
\text{photon}: \quad & k_1 = (E_{k_1}, \boldsymbol{k}_1) = (k, 0, 0, k), \\
\text{nucleon}: \quad & p_1 = (E_{p_1}, \boldsymbol{k}_2) = (\sqrt{k^2 + M_N^2}, 0, 0, -k), \\
\bar{D}^* \text{ meson} \quad & k_2 = (E_{k_2}, \boldsymbol{p}_1) = (\sqrt{p^2 + M_{D^*}^2}, p\sin\theta, 0, p\cos\theta), \\
Y_c \text{ hyperon}: \quad & p_2 = (E_{p_2}, \boldsymbol{p}_2) = (\sqrt{p^2 + M_{Y_c}^2}, -p\sin\theta, 0, -p\cos\theta).
\end{aligned} \tag{9}$$

The transverse and longitudinal polarization vectors for the outgoing $\bar{D}^*$ meson are assigned as follows:

$$\begin{aligned}
&\epsilon_{2,x} = (0, \cos\theta, 0, -\sin\theta), \quad \epsilon_{2,y} = (0, 0, 1, 0), \\
&\epsilon_{2,z} = \frac{E_{k_2}}{(p^2 + E_{k_2}^2)^{1/2}} \left(\frac{p}{E_{k_2}}, \sin\theta, 0, \cos\theta \right).
\end{aligned} \tag{10}$$

REFERENCES

[1] A. V. Berezhnoy, V. V. Kiselev and A. K. Likhoded, arXiv:hep-ph/9901333.

[2] J. Breitweg *et al.*, Eur. Phys. J. C **6**, 67 (1999).

[3] E. Tomasi-Gustafsson and M. P. Rekalo, Eur. Phys. J. A **21**, 469 (2004)..

[4] M. Tanabashi *et al.*, Phys. Rev. D **98**, 030001 (2018).

[5] W. Cassing, L. A. Kondratyuk, G. I. Lykasov and M. V. Rzjanin, Phys. Lett. B **513**, 1 (2001).

[6] S. Filipponi, G. Pancheri and Y. Srivastava, Phys. Rev. Lett. **80**, 1838 (1998).

[7] M. Guidal, J. M. Laget and M. Vanderhaeghen, Nucl. Phys. A **627**, 645 (1997).

[8] V. G. J. Stoks and T. A. Rijken, Phys. Rev. C **59**, 3009 (1999.

[9] S. H. Kim, S. i. Nam, A. Hosaka and H. C. Kim, Phys. Rev. D **88**, 054012 (2013).